ISSN 1674-1056
http://cpb.iphy.ac.cn
http://iopscience.iop.org/cpb
中国物理 B
Chinese Physics
中国物理 Chinese Physics B

Light-scattering model for aerosol particles with irregular shapes and inhomogeneous compositions using a parallelized pseudo-spectral time-domain technique

Shuai Hu(胡帅), Taichang Gao(高太长), Hao Li(李浩), Lei Liu(刘磊), Ming Chen(陈鸣), Bo Yang(杨波)
Citation: Chin. Phys. B . 2018, 27(5): 054216. **doi:** 10.1088/1674-1056/27/5/054215

Journal homepage: http://cpb.iphy.ac.cn; http://iopscience.iop.org/cpb

What follows is a list of articles you may be interested in

Difference scattering field properties between periodic defect particles and three-dimensional slightly rough optical surface

Cheng-Xian Ge(葛城显), Zhen-Sen Wu(吴振森), Jing Bai(白靖), Lei Gong(巩蕾)
Chin. Phys. B . 2017, 26(6): 064201. **doi:** 10.1088/1674-1056/26/6/064201

Theoretical studies on particle shape classification based on simultaneous small forward angle light scattering and aerodynamic sizing

Jin-Bi Zhang(张金碧), Lei Ding(丁蕾), Ying-Ping Wang(王颖萍), Li Zhang(张莉), Jin-Lei Wu(吴金雷), Hai-Yang Zheng(郑海洋), Li Fang(方黎)
Chin. Phys. B . 2016, 25(3): 034201. **doi:** 10.1088/1674-1056/25/3/034201

A new kind of superimposing morphology for enhancing the light scattering in thin film silicon solar cells：Combining random and periodic structure

Huang Zhen-Hua, Zhang Jian-Jun, Ni Jian, Wang Hao, Zhao Ying
Chin. Phys. B . 2014, 23(8): 084205. **doi:** 10.1088/1674-1056/23/8/084205

Measurements of NO_2 mixing ratios with topographic target light scattering-differential optical absorption spectroscopy system and comparisons to point monitoring technique

Wang Yang, Li Ang, Xie Pin-Hua, Zeng Yi, Wang Rui-Bin, Chen Hao, Pei Xian, Liu Jian-Guo, and Liu Wen-Qing
Chin. Phys. B . 2012, 21(11): 114211. **doi:** 10.1088/1674-1056/21/11/114211

Electromagnetic scattering of the carbon nanotubes excited by an electric line source

Wang Yue, Wu Qun, Wu Yu-Ming, He Xun-Jun, Li Le-Wei
Chin. Phys. B . 2012, 21(1): 014212. **doi:** 10.1088/1674-1056/21/1/014212

Structural, vibrational, optical, photoluminescence, thermal, dielectric, and mechanical studies on zinc (tris) thiourea sulfate single crystal: A noticeable effect of organic dye*

Mohd Shkir[1,†], V Ganesh[1], S AlFaify[1,‡], I S Yahia[1], and Mohd Anis[2]

[1] *Advanced Functional Materials & Optoelectronic Laboratory, Department of Physics, Faculty of Science, King Khalid University, Abha* 61413, *Saudi Arabia*

[2] *Department of Physics, Sant Gadge Baba Amravati University, Amravati* 444602, *Maharashtra, India*

(Received 7 December 2017; revised manuscript received 22 January 2018; published online 26 April 2018)

In this work, uranine-dyed zinc (tris) thiourea sulfate (ZTS) monocrystals, 26 mm×15 mm×10 mm in size, were synthesized by the solution method at ambient temperature. Their purity, crystallinity, lattice parameters, and functional modes were studied by x-ray diffraction, Fourier transform-infrared spectroscopy (FT-IR), and FT-Raman spectroscopy analyses. The sodium ion content of the crystals from the dye was confirmed by elemental analysis. The diffused reflectance spectral analysis of the dyed crystal revealed a characteristic absorption band at 490 nm attributed to the presence of the dye. The calculated band gaps of the non-dyed and dyed crystals were 4.53 and 4.57 eV, respectively. A green emission peak at $\sim (512 \pm 4)$ nm was observed in the photoluminescence spectrum of the uranine-dyed crystals. A differential scanning calorimetry study confirmed that the thermal stability improved owing to the addition of the dye. Dielectric and microhardness studies were conducted to examine the significant improvements in the corresponding properties of dyed crystals. The results demonstrated the competency of the dyed ZTS crystals for applications in optoelectronic devices.

Keywords: crystal growth, dielectric properties, luminescence, thermal properties, mechanical properties

PACS: 42.70.Mp, 77.84.–s, 42.72.Bj, 74.25.Jb **DOI:** 10.1088/1674-1056/27/5/054216

1. Introduction

Thus far, nano to macroscale materials have undergone significant developments in the field of nonlinear optics owing to their extensive applications in advanced devices. Specifically, single crystals with good nonlinear optical (NLO) properties are in demand for applications in optical communication, data storage, and optoelectronic and photonic devices.[1–10] Therefore, compatible NLO materials for designing and optimizing modern technological devices were commercialized and functionalized on a large scale. A family of NLO thiourea metal complex crystals have attracted immense attention from researchers owing to their mutual properties between organic and inorganic counterparts.[11,12] Among these, zinc (tris) thiourea sulfate (ZTS) is a well-recognized non-centrosymmetric material with good structural, electrical, and linear–nonlinear optical properties, birefringence, and high tolerance to laser power.[13] Furthermore, ZTS is a stable semi-organic complex crystallized in an orthorhombic crystal structure with the space group $Pca2_1$.[14] Since its invention in 1968 by Andreetti *et al.*,[14] researchers have been attempting to enhance its structural and physical properties using various organic and inorganic additives or dopants.[15–23] These studies revealed that ZTS crystals can supplant the KDP crystal for manufacturing laser-assisted high-power photonic devices.[24] In the last few decades, organic-dye-doped single crystals have been grown for their applications in optoelectronics and solid state lasers.[20,25–36] Such applications necessitate the development of dyed single crystals of organic, inorganic, and semi-organic materials. Hitherto, reports on amaranth, titan yellow, and brilliant green dye-doped/-added ZTS crystals have been scarce.[20,37] Moreover, there are no growth and characterization studies on fluorescein sodium salt (FNa)- or uranine (U) (a p-type organic semiconductor)-dyed ZTS single crystals. Therefore, in this work, our group first attempted to grow large single crystals of U-dyed ZTS (UZTS) crystals. The grown crystals were systematically investigated by powder x-ray diffraction (PXRD), Fourier-transform infrared (FT-IR), FT-Raman, ultraviolet-visible-near infrared (UV-vis-NIR) diffuse reflectance, photoluminescence (PL) spectroscopies, and dielectric characterization.

2. Experimental procedure

2.1. Monocrystal growth

Pure and dyed ZTS $[C_3H_{12}N_6O_4S_4Zn]$ crystals were synthesized by mixing zinc sulfate heptahydrate $[ZnSO_4{\cdot}7H_2O]$

*Project supported by the Fund from the Deanship of Scientific Research at King Khalid University, Saudi Arabia (Grant No. R.G.P.2/9/38).

†Corresponding author. E-mail: shkirphysics@gmail.com

‡Corresponding author. E-mail: sasaalfaify@hotmail.com

© 2018 Chinese Physical Society and IOP Publishing Ltd

and thiourea [$CS(NH_2)_2$] in 1:3 stoichiometric ratio in two separate glass pots following a previous procedure.[38] The pure sample was untreated, while in the dyed sample, 0.1 wt% uranine [$C_{20}H_{10}Na_2O_5$] ($\sim 9.663 \times 10^{-4}$ g of uranine dye in 1 g of ZTS) was added and continuously stirred at $\sim$ 320 K. Both samples were then dissolved in deionized water and recrystallized at room temperature to achieve a high-purity material for the optimized growth of single crystals. The filtrates of the prepared solutions were transferred into their corresponding beakers, roofed with a perforated sheet, and immersed in a steady-temperature bath at (27 ± 1) °C. Single crystals of UZTS ($\sim$ 26 mm$\times$15 mm$\times$10 mm) were harvested from the parent solution after 30 days as shown in Fig. 1(a). Furthermore, the dyed ZTS crystals were grown mainly along the [100] direction, consistent with that reported for pure ZTS crystals.[38] The images of the sliced and polished crystal specimens from the bulk crystal are depicted in Figs. 1(b) and 1(c), and were used for further analyses. Observably, the grown crystals were highly transparent, and thus, suitable for optoelectronic applications.

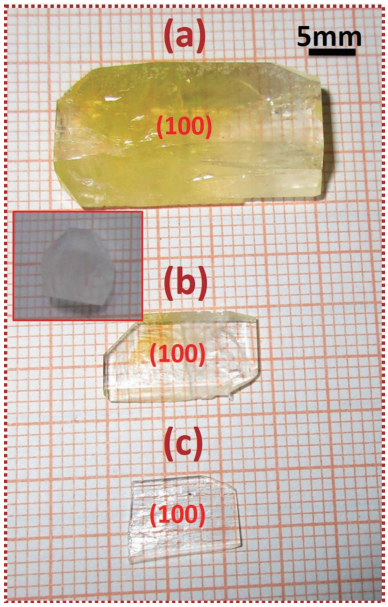


Fig. 1. (a) As-grown and ((b), (c)) sliced and polished single crystals of UZTS.

2.2. Characterization methods

For crystal structure and lattice parameters analyses, the grown crystals were subjected to PXRD measurement using a Shimadzu X-600 x-ray diffractometer with CuK_α radiation (40 kV, 30 mA, $\lambda = 0.1543$ nm) at a scan rate of 2°/min over an angular range of 5°–70°. Furthermore, energy-dispersive x-ray spectroscopy (EDXS) analysis with scanning electron microscopy (SEM) was performed using a JSM 6360 LA (JEOL, Japan) to confirm the presence of the dopant in the ZTS crystals. Vibrational studies were conducted with FT-IR and FT-Raman spectroscopies using THERMO SCIENTIFIC, DXR DT-IR, and FT-RAMAN spectrophotometer (Waltham, Massachusetts, USA). For optical analysis, a Shimadzu UV-vis-NIR spectrophotometer model (UV-3600) (Kyoto, Kyoto Prefecture, Japan) was employed to record the diffuse reflectance (DR) within 190–1000 nm. The room-temperature PL spectrum was recorded using a Lumina Fluorescence Spectrometer (Thermo Fisher Scientific, USA) at different excitation wavelengths. Thermal analysis was accomplished by differential scanning calorimetry (DSC) 60 (C30455001206SA) at a heating rate of 15 °C/min over the temperature range of 30–300 °C. The prepared samples were sputter-coated on both sides for dielectric measurement with a KEITHLEY 4200-SCS system (Keithley (a Tektronix company, USA). The dielectric constant, dielectric loss, and alternate current (AC) conductivity were obtained over a high-frequency range of 1 kHz to 10 MHz.

3. Results and discussion

3.1. XRD and EDX analyses

Figure 2 shows the recorded PXRD pattern with *hkl* indexing for the pure and dyed ZTS crystalline powder specimens. The peak intensities of the dyed ZTS crystals were enriched, which signifies the enhancement in the quality of the crystal. For further structural analysis, the recorded diffraction data were outsourced from POWDERX software (http://www.ccp14.ac.uk/tutorial/powderx/). The crystal system was orthorhombic, belonging to the $Pca2_1$ space group, with unit cell dimensions of $a = 11.120$ Å, $b = 7.770$ Å, $c = 15.490$ Å, and $V = 1338.37314$ Å; and $a = 11.121$ Å, $b = 7.771$ Å, $c = 15.493$ Å, and $V = 1338.789$ Å^3 for the pure and dyed ZTS crystals, respectively, which agrees with earlier reported data.[14] The c value and, effectively, the volume, increased due to the presence of the dye in the ZTS crystal lattice. Upon close inspection of the diffraction pattern, shifts in the peak positions were observed, as depicted in Fig. 2(b). Evidently, the diffraction peaks of the dyed specimen shifted toward the lower angle, which signifies the interaction of uranine dye with the ZTS crystalline matrix. The presence of the uranine dye phase was confirmed by the appearance of low-intensity XRD peaks 33.48°$(50\bar{2})$, 36.12°$(24\bar{3})$, 37.82°(423), and 40.36°(225) (JCDPS card No. #51-2376)[39] in the spectrum of the dyed crystals (Fig. 2(c)). This was further supported by the EDX spectrum as shown in Fig. 2(d). Moreover, evidence of sodium ions in the ZTS matrix from its interaction with uranine dye was observed. Thus, we successfully prepared uranine-dyed ZTS crystals.

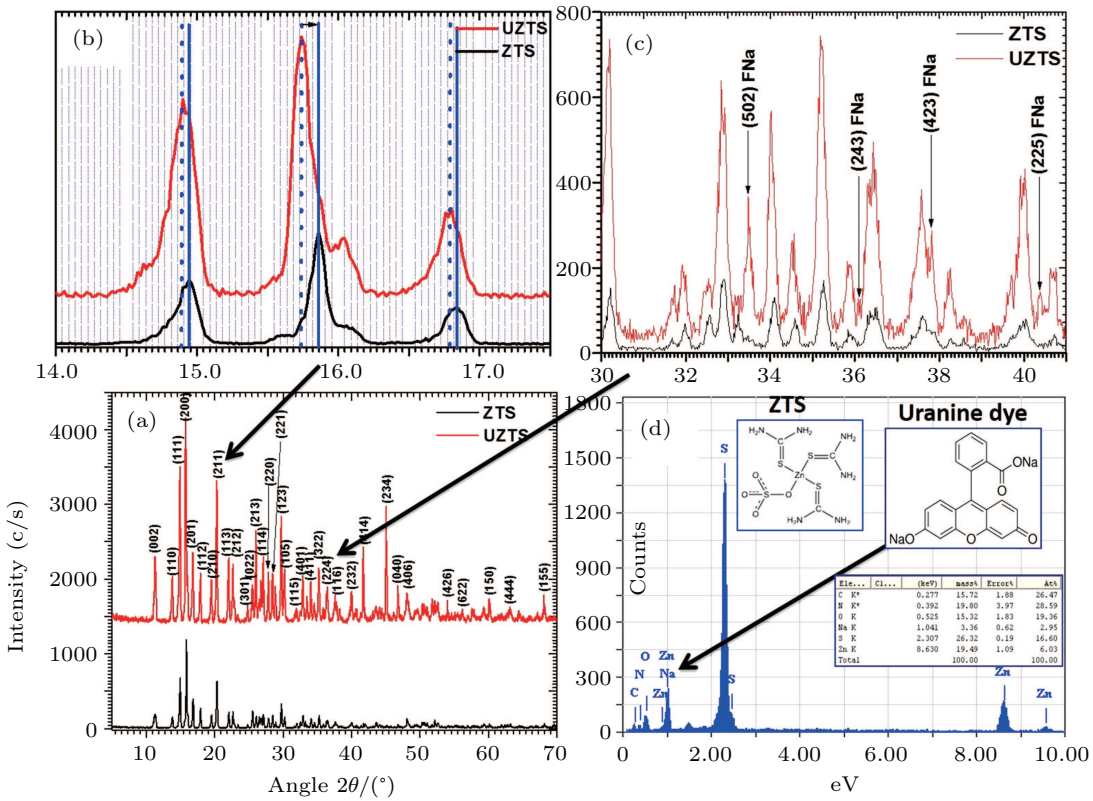


Fig. 2. (a) Indexed x-ray diffraction patterns, (b) magnified view of high-intensity peaks, (c) magnified view of dye peaks, and (d) EDX spectrum of UZTS crystals.

3.2. FT-IR and FT-Raman analyses

For the vibrational studies, the FT-IR and FT-Raman spectra of the grown crystals were recorded over the wavenumber ranges of 4000 to 400 cm^{-1} and 1800 to 50 cm^{-1} (main), respectively, as shown in Figs. 3(a) and 3(b). Symmetric and asymmetric NH stretching vibrations of several N–H–O bonds in ZTS were observed in the higher wavenumber region (i.e., 3000–3500 cm^{-1}). All IR and Raman vibration modes, and their corresponding assignments are presented in Table 1. Clearly, almost all the peak positions are slightly shifted, due to the interaction of the dye with the ZTS matrix. Furthermore, the intensities of the Raman peaks were observably enhanced due to doping. Therefore, improvement in the luminescence properties of the ZTS crystals is expected.

Table 1. Calculated mechanical parameters for pure and dyed ZTS crystals.

Crystal	H_v/kg·mm^{-2}	Meyer's law (Meyers No.)	Hays–Kendall approach			PSR model		
			W/g	A_1	H_o/kg·mm^{-2}	a	b	H_o/kg/mm^{-2}
ZTS	122	2.45	–10.82	0.073	135.3	–9.32	0.095	176.1
UZTS	192	2.63	–15.63	0.1152	213.6	–20.26	0.114	211.4

Figures 3(a) and 3(b) reveal a broad envelope between 1700 and 3000 cm^{-1} due to the symmetric and asymmetric modes of NH_2 in zinc-coordinated thiourea molecules. The strong bands at 1633 cm^{-1} in the pure crystal spectrum and at 1632 cm^{-1} in the UZTS crystal spectrum both correspond to the plane bending vibration of NH_2. The stretching vibration modes of N–C–N bonds were observed at 1517 and 1540 cm^{-1}, and at 1515 and 1539 cm^{-1} in pure and UZTS crystal spectra, respectively. The vibration bands observed at 1442 and 1403 cm^{-1}, and at 1440 and 1404 cm^{-1} in the IR spectra of ZTS and UZTS correspond to the asymmetric stretching of CN and stretching of CS bonds, respectively. The coordination of zinc with thiourea through sulfur was confirmed by the presence of C = S vibration bands at 1089 cm^{-1} in the spectra of both crystals.

The vibration bands at 1411 and 730 cm^{-1} attributed to the C=S stretching vibration of thiourea were shifted toward lower wavelengths of 1410 and 716 cm^{-1} in the ZTS spectrum, and 1403 and 710 cm^{-1} in the UZTS spectrum, respectively, indicating the interaction of the dye with the pure material. The respective stretching vibrations of SO_4 and NH_2 at 1112 and 1093 cm^{-1} in the ZTS spectrum, were slightly shifted to 1107 and 1086 cm^{-1} in the UZTS spectrum, respectively. Similarly, vibration bands assigned to S=C–N and SO_4 vibrations at 1035 and 957 cm^{-1}, respectively, in the ZTS spectrum, were observed at 1024 and 947 cm^{-1} in the UZTS spectrum, suggesting the interaction of sulfur with the dye. The symmetric stretching and rocking vibrations of C–N at

$\sim$ 716, 478, 607, and 432 cm^{-1} in the spectrum of pure crystals were shifted to 710, 481, 609, and 426 cm^{-1} in that of the doped samples, respectively. The vibrational band assigned to Zn–S at 271 cm^{-1} in the ZTS spectrum was observed at 263 cm^{-1} in the UZTS spectrum.[36] Furthermore, the vibrational peaks at 241 and 182 cm^{-1} in the ZTS spectrum and at 233 and 173 cm^{-1} in the UZTS spectrum were attributed to lattice vibrations. These vibrational modes concur with previous reports on pure and dyed ZTS.[20,40–42] The position of the vibration bands and their intensities were shifted and enhanced, respectively, because of the interaction of the dye with the ZTS crystal.

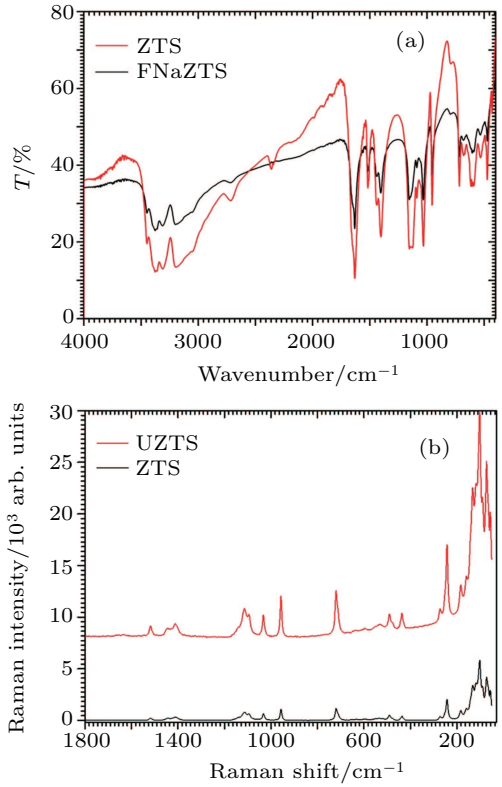


Fig. 3. (a) FT-IR and (b) FT-Raman spectra for pure and dyed ZTS crystals.

3.3. Optical studies

3.3.1. Diffuse reflectance (DR) analysis

To study the impact of the p-type organic semiconductor dye on the optical properties of ZTS, the DR spectrum was recorded as shown in Fig. 4(a). For this, the crystals were crushed for a similar duration using a mortar to obtain a fine and homogeneous powder. The powder was then sieved through a sample holder ($\sim$ 2 mm). The DR spectrum was analyzed using the Kubelka–Munk theory.[43] From Fig. 4(a), it is evident that the cut-off wavelength for the pure crystal is slightly reduced from 294 to 292 nm for the dyed crystal. An absorption band at 490 nm was observed in the spectrum of the dyed crystal but was absent in that of the pure crystal, which signifies the interaction of the dye with the ZTS crystalline matrix. A similar absorption band was observed previously in the spectrum of dyed ZTS crystals.[20,21] Previously, non-uniform dye-doping of the ZTS crystalline matrix was reported.[20] Similarly, the dye herein also interacts almost heterogeneously with ZTS (Fig. 1). Furthermore, the optical band gap energy of the grown crystals was determined based on the Kubelka–Munk relation[43]

$$F(R) = \frac{(1-R)^2}{2R}, \tag{1}$$

where $F(R)$ is Kubelka–Munk function, and R is the absolute reflectance.

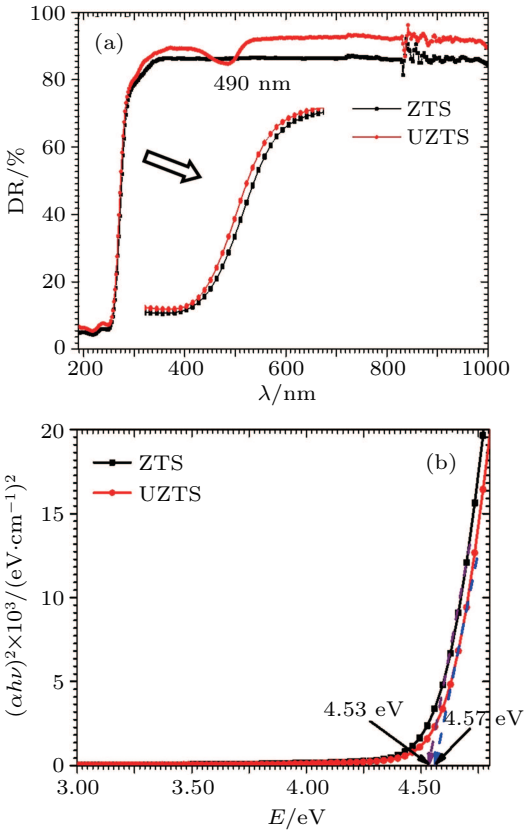


Fig. 4. (a) Diffused reflectance spectra and (b) plots of optical band gap.

The absorption coefficient, α, in terms of $F(R)$ is

$$\alpha = \frac{\text{absorbance}}{s} = \frac{F(R)}{s}. \tag{2}$$

Finally, the optical band gap energy is calculated from the following equation:

$$(\alpha h\upsilon)^{1/n} = \left(\frac{F(R)h\upsilon}{s}\right)^{1/n} = A\left(h\upsilon - E_g\right), \tag{3}$$

where n is an index value which explains the route of optical absorption,[44] and constants, A, h, and υ are the parameter for transitions, Planck's constant, and frequency of the incident photon, respectively. The band gap energies of both crystals were determined for all the transition values of n. However, the best-fitted curve was realized at $n = \frac{1}{2}$ for both crystals, which corresponds to a directly allowed transition. The plot of

the variation of $(\alpha h\upsilon)^2$ with $h\upsilon$ is shown in Fig. 4(b), and the value of the energy gap was derived from the $x(h\upsilon)$-intercept, where $(\alpha h\upsilon)^2 = 0$. The band gap energies were 4.53 and 4.57 eV for pure and dyed ZTS crystals, respectively. These confirm the enhancing effect of uranine dye on the band gap energy of the ZTS crystal as observed previously.[20,45] The higher band gap energy suggests that ZTS crystals are very useful in optoelectronic devices.[3,9,46,47]

3.4. Photoluminescence (PL) study

The PL study involves the evaluation of the trajectory of electron transition due to photo-excitation in the given energy states of the material, effectively probing the associated recombination rate and electronic purity of the material.[48–50] Figures 5(a), 5(b), and 5(c) show the recorded PL spectra of the grown crystals at room temperature under different excitation wavelengths. The emission spectra of the dyed crystals were recorded under excitation wavelengths of ∼ 310, 358, and 385 nm. Accordingly, the spectra of the pure ZTS crystal possess only one emission band at ∼ 348, 409, and 442 nm, under each respective excitation wavelength, along with a few low-intensity bands between 360 and 470 nm. The spectrum of the dyed single crystal exhibits an intense UV emission band at 346 nm and low-intensity violet-blue/blue bands at ∼ 420 and 445 nm when excited at 310 nm. Correspondingly, these bands were observed at ∼ 408 (intense), 448, and 459 nm, and 440 (intense), 460 nm under excitation wavelengths of ∼ 358 and 385 nm, respectively. Furthermore, a strong green emission band at ∼ 511, 508, and 512 nm appeared under each respective excitation wavelength. This new emission band might have resulted from the presence of uranine dye in the ZTS matrix. An emission band at ∼ 528 nm was observed in our previous report on ZTS crystals with titan yellow dye.[37] However, it may have shifted toward a lower wavelength due to the presence of uranine dye. The appearance of luminescence bands at 408 and 416 nm could be attributed to the presence of intrinsic defects.[52,53] The luminescence band at $\sim 448 \pm 12$ nm was induced by increased S^{2-} vacancies[54] or zinc interstitials.[55] This band was previously observed at 434 nm in ZTS and 433 nm in TYZTS.[37] Moreover, previous reports on pure and dyed ZTS crystals documented luminescence bands at 348 and 416 nm ($\lambda_{exc} = 310$ nm), 423 nm ($\lambda_{exc} = 358$ nm), and 406 nm ($\lambda_{exc} = 249$ nm) with a broad emission band between 370–500 nm.[20,53,56] The current PL study demonstrates the tremendous potential of UZTS crystals for applications in biochemical/biomedical systems for the detection of compounds.[57]

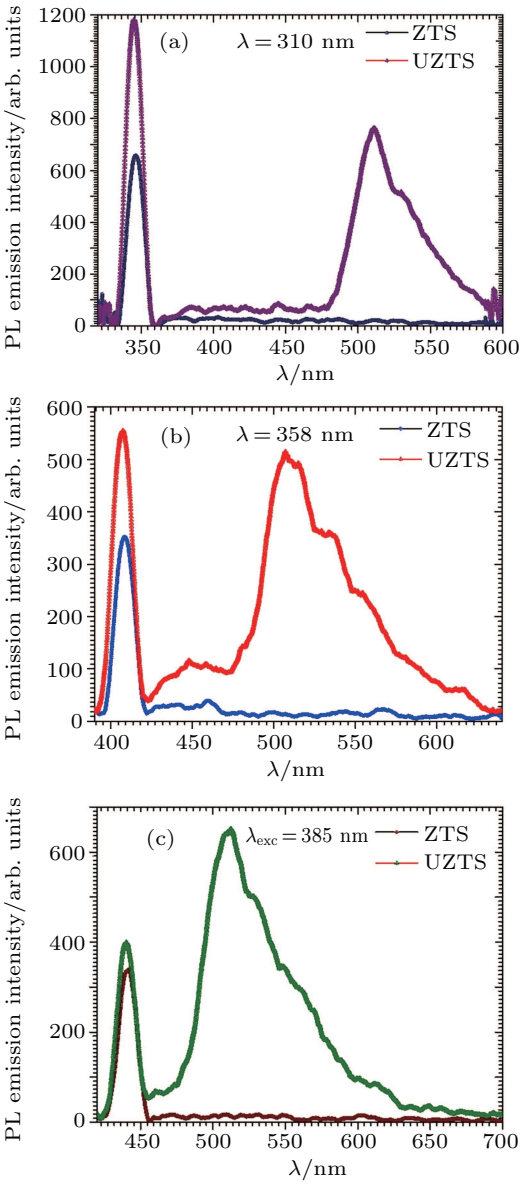


Fig. 5. PL emission spectra of UZTS crystals at excitation wavelengths of (a) 320 nm, (b) 358 nm, and (c) 385 nm.

3.5. Thermal analysis

Figures 6(a) and 6(b) show the recorded DSC curves for non-dyed and dyed ZTS crystals, respectively. DSC is an excellent tool for thermal study and provides accurate information on the thermal stability of any material, suggesting its application in nonlinear devices. Here, the influence of the dye on the thermal behavior of ZTS crystal was studied. Figure 6 shows that both pure and dyed ZTS crystals possess good thermal stability. Furthermore, upon melting, both crystals did not exhibit any weight loss from water evaporation, as water was the solvent for crystal growth. The performance of the prepared samples was described by the sharpness of the DSC peaks. The endothermic peaks of the ZTS and UZTS crystals were observed at 241 and 243 °C, respectively. Both crystals were stable up to these temperatures, which correspond to their melting point. Evidently, the melting point of ZTS improved by ∼ 2 °C due to uranine dye doping. The melting

points of pure and dyed ZTS crystals were higher and comparable with that of organic, semi-organic, inorganic, and metal-organic materials.[58–63]

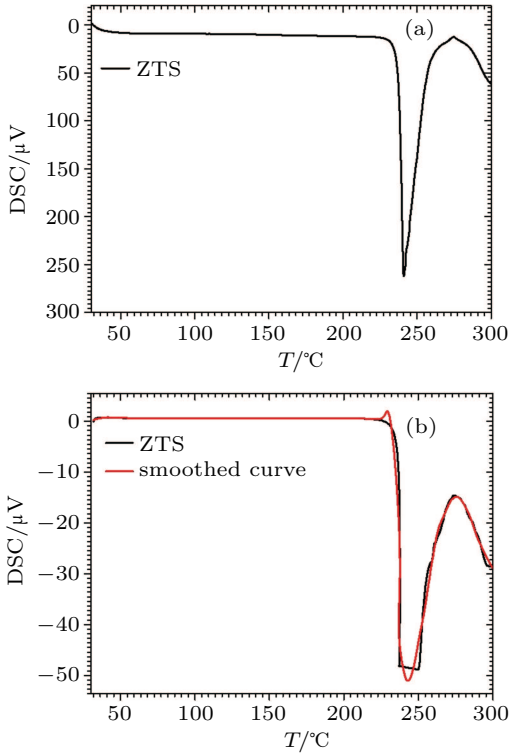


Fig. 6. DSC curves for (a) pure and (b) dyed ZTS crystals.

3.6. Dielectric constant and ac electrical conductivity analyses

Dielectric materials are widely used in optoelectronic devices, because the dielectric constant is directly related to the refractive index and poling voltage. A low dielectric constant reduces the discrepancy in refractive index and facilitates low poling voltage. For dielectric and electrical conductivity analyses, we measured the capacitance (C), loss tangent ($\tan\delta$), and impedance (Z) of the crystals. The dielectric constant (ε') was calculated from the equation: $\varepsilon' = \frac{Ct}{\varepsilon_0 A}$, where t is the thickness of the sample, ε_0 is vacuum permittivity, and A is the area of electrodes. Using the values of ε', the dielectric loss (ε'') was evaluated with the equation: $\varepsilon'' = \tan\delta \times \varepsilon'$. Figure 7(a) plots the variations of ε' and ε'' with frequency. It also reveals that the value of the dielectric constant is higher in the low-frequency region and significantly decreases with increasing frequency but stabilizes at a certain point. The high dielectric constant at low frequency is attributed to electronic, ionic, dipolar, and space-charge polarizations,[64,65] while the low and stable value at higher frequency is a consequence of the minimal contribution from the above mentioned polarizations. The low dielectric constant of the dyed crystal validates its applications in photonics, second-harmonic generation (SHG), and NLO devices.[66] The value of ε' for the ZTS crystals was enhanced with uranine dye, and was higher than the previously reported values of pure and dyed ZTS crystals.[20,51] Based on Fig. 7(a), the dielectric loss also follows a similar trend as it decreases with frequency. Consequently, a very low value was attained, which indicates that the grown crystals contain small amounts of defects. Therefore, they exhibit good optical quality and are desirable in nonlinear optical applications.[67] The total AC conductivity ($\sigma_{\text{ac.tot.}}$) was evaluated through the equation: $\sigma_{\text{ac.tot.}} = \frac{t}{Z \times A}$. Its variation with frequency is illustrated in Fig. 7(b). Observably, the value of $\sigma_{\text{ac.tot.}}$ increases with frequency and follows a universal frequency power law. The conductivity mechanism in the grown crystals was analyzed using the Jonscher Law:[68] $\sigma_{\text{ac.tot.}} = \sigma_{\text{dc}} + B\omega^s$, where σ_{dc}, B, and ω represent the direct current conductivity, a constant, and angular frequency, respectively, and s is the exponent of frequency. The value of s was determined from the slope of $\ln\sigma_{\text{ac.tot.}}$ vs. $\ln\omega$ (Fig. 7(b)) to be 1.0227 with a standard error of 0.1044. Its value less than unity (~ 0.9183) was associated with the lack of measurable direct current conductivity. Hence, the hopping mechanism in the crystals involved translational motion with sudden hopping. These findings show that the values of ε', ε'', and $\sigma_{\text{ac.tot.}}$ of ZTS can be tuned with the addition of uranine.

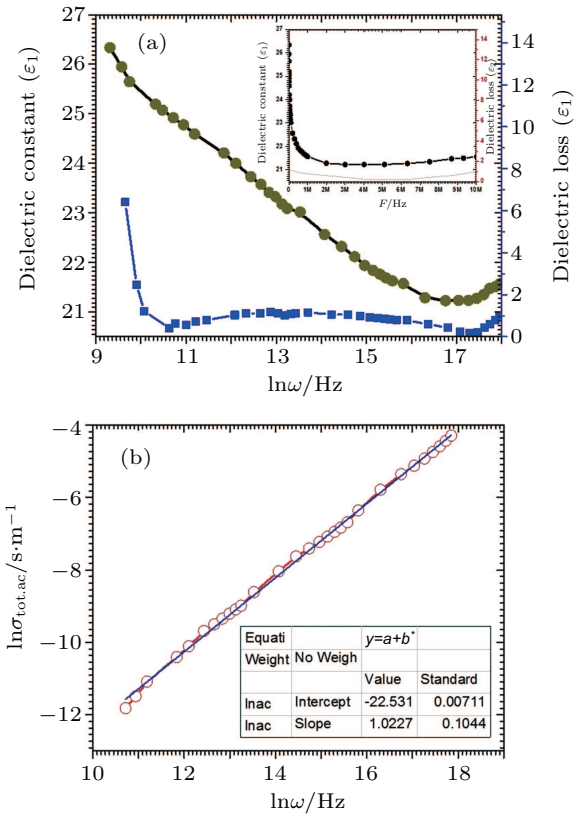


Fig. 7. Plots of (a) ε' and ε'' versus $\ln\omega$ and (b) $\ln\sigma_{\text{ac.tot.}}$ versus $\ln\omega$.

3.7. Mechanical studies

The hardness of the single crystal is affected by the Debye's temperature, lattice energy, heat of formation, and in-

teratomic bonding, which are also important in studying various strength parameters.[69,70] The indentation technique is a simple but unique method to examine different properties, e.g., normal indentation size effect (NISE), reverse indentation size effect (RISE), yield point of fracture, and brittleness.[71] Therefore, to study the effect of load on the (100) plane of pure and UZTS crystals, Vicker's indentation test was performed over the load range of 10–100 g. To calculate the different strength parameters of the crystals, 26 mm×15 mm×10 mm samples were prepared, load tested, and evaluated using the following relation:

$$H_{\rm V} = 1.854P/d^2, \tag{4}$$

where P is the applied load in kg, and d is the indentation diagonal length in μm. The effect of load on hardness is shown in Fig. 8(a). Evidently, the hardness increased with the indentation load. This is attributed to the enhanced gliding of slip planes and the value of the corresponding constant at higher load, which result from the pinning of dislocations and their interaction with each other. This behavior is presented by RISE, which is also observed in pure and doped materials.[72] To understand RISE in pure and UZTS crystals, standard models were selected and discussed herein.

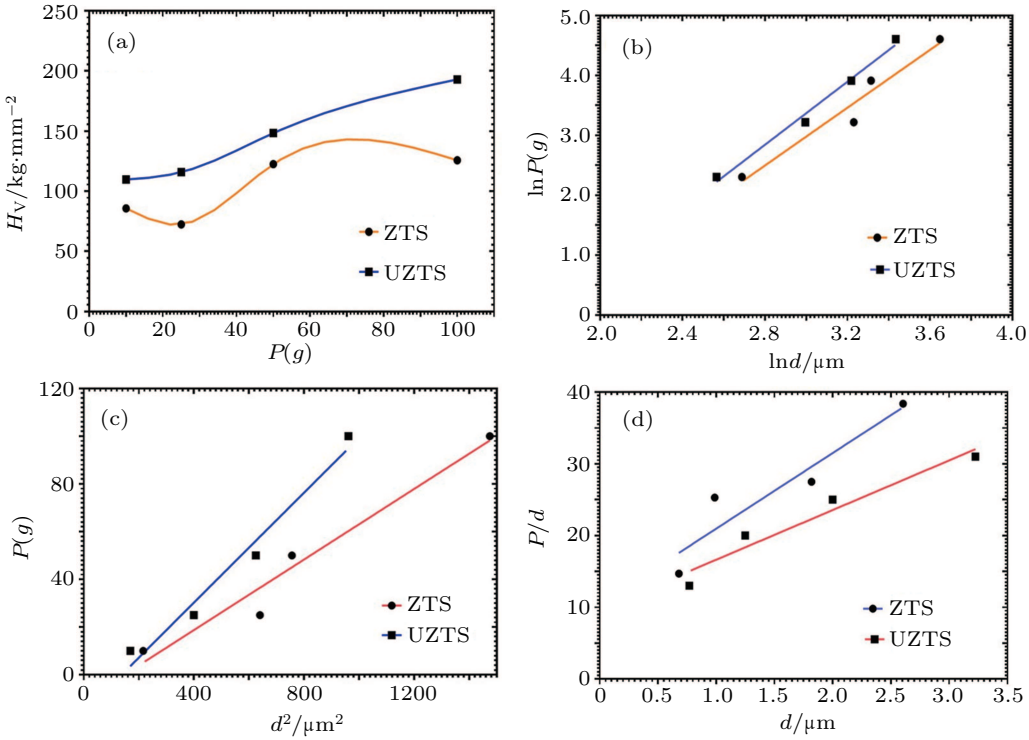


Fig. 8. Plots of (a) $H_{\rm V}$ versus P, (b) ln$P$ versus ln$d$, (c) P versus d^2, and (d) P/d versus d.

3.7.1. Meyer's law

Meyer's law describes RISE in crystals by the following relation:[73]

$$P = ad^n, \tag{5}$$

where P is the applied load, d is the diagonal length of the indentation mark, a is a constant for any given material, and n is the Meyer index or work hardening coefficient. Here, the n values were calculated from the slope of ln$P$ vs. ln$d$ plots (Fig. 8(b)). The corresponding values for pure and UZTS crystals are given in Table 1. Consequently, samples with higher values of n, i.e., $n > 2$, exhibit RISE. This trend was intensively discussed in previous studies.[72,74] However, Meyer's law is suitable only for setups with lower loads. To compensate for this, we implemented Hays–Kendall's law.

3.7.2. Hays–Kendall's law

According to Hays–Kendall's law, the relation between the applied load, P, and the indentation diagonal, d, is given by[64]

$$P = W + A_1 d^2, \tag{6}$$

where W is the minimum load required for plastic deformation, and A_1 is a load-independent coefficient.[75,76] The plots of P versus d^2 (Fig. 8(c)) provide the values of W and A_1, which are listed in Table 1. Using the values of A_1, the corrected hardness, $H_{\rm o}$, is calculated using the equation $H_{\rm o} = 1854A_1$. With this approach, several reports suggest that the positive values of w imply NISE, while negative values signify RISE.[72] Here, pure and UZTS crystals both yielded negative values, indicating the existence of RISE. Furthermore, to understand the RISE at load-independent and dependent regions, the proportional specimen resistance (PSR) model was

adopted.

3.7.3. Proportional specimen resistance (PSR) model

According to the PSR model,[74,76] the load, P, and indentation diagonal, d, are related by

$$P = ad + bd^2, \tag{7}$$

where a is the frictional resistance developed at the indenter-specimen interface, and b is the load-independent constant. These values were obtained from the P/d versus d (Fig. 8(d)) plots. In literature, materials with $a > 0$ undergo NISE, while those with $a < 0$ experience RISE. Presently, both samples have $a < 0$, which indicates the presence of RISE. Moreover, the load-independent hardness was also calculated using the equation, $H_o = 1854b$,[74] the results for which are presented in Table 1.

4. Conclusion

Single crystals of UZTS, 26 mm×15 mm×10 mm in size, were synthesized within 30 days by the solvent evaporation method. The effect of uranine dye on the crystal morphology and color of the ZTS crystal was investigated. A yellow crystal of ZTS was obtained when grown with uranine dye. XRD analysis illustrated slight shifts in the diffraction peak positions and lattice parameters. The observed shift in vibrational modes confirmed the presence of the dye and its interaction with the ZTS crystal matrix. Furthermore, quantitative and qualitative analyses performed by EDXS measurements confirmed the presence of Na^+ (associated with uranine dye) in ZTS. The low optical absorbance and high reflectance of the samples indicate that they are optically transparent. The interaction of the dye with ZTS was also evidenced by a new absorption band at $\sim$ 490 nm in the DR spectrum of UZTS. The optical band gap energies of ZTS and UZTS were calculated using the Kubelka–Munk model to be 4.53 and 4.57 eV, respectively. Both crystals possess very high band gap, which makes them useful in optoelectronic applications. PL emissions were recorded at three excitation wavelengths. The PL spectra of pure ZTS showed one intense emission band at $\sim$ 346, 409, and 442 nm, respectively, when excited under λ_{ex} = 310, 358, and 385 nm. However, for the dyed ZTS crystals excited under the same wavelengths, two major emission bands were observed in their spectra at $\sim$ 345 and 511 nm ($\lambda_{ex} = 310$ nm), $\sim$ 408 and 508 nm ($\lambda_{ex} = 358$ nm), and $\sim$ 440 and 512 nm ($\lambda_{ex} = 385$ nm). Furthermore, an evident PL band at $\sim (508 \pm 4)$ nm was observed in the spectrum of the UZTS corresponding to its content of uranine dye. The thermal stability (i.e., melting point) of UZTS improved as reflected by the increase in the melting point from 241 to 243 °C. The high dielectric constant and low dielectric loss of the samples revealed a low defect content in them. The total AC conductivity was observed to increase with frequency. The s value of the crystals indicated the existence of the hopping mechanism, which involves translational motion with sudden hopping. The mechanical properties of the UZTS crystals improved compared to those of pure crystals.

References

[1] Bafandeh N, Larijani M M, Shafiekhani A, Hantehzadeh M R and Sheikh N 2016 *Chin. Phys. Lett.* **33** 117801
[2] Han W, Li D Z, Xiang Y, Tian Y, Wang F, Li F Q, Wang L Q, Feng B, Zhao J P, Zheng K X, Zhu Q H, Wei X F, Zheng W G and Gong M L 2016 *Chin. Phys. Lett.* **33** 27803
[3] Dai L, Liu C R and Tan C 2017 *Chin. Phys. B* **26** 44207
[4] Shaikh R N, Anis M, Shirsat M D and Hussaini S S 2018 *Optik* **154** 435
[5] Saleh B and Teich M C 1991 *Fundamentals of Photonics* (New York: John Wiley & Sons)
[6] Penn B G, Cardelino B H, Moore C E, Shields A W and Frazier D 1991 *Prog. Cryst. Growth CH.* **22** 19
[7] Shakir M, Singh B, Kumar B and Bhagavannarayana G 2009 *Appl. Phys. Lett.* **95** 252902
[8] Shakir M, Kushwaha S, Maurya K and Bhatt R 2010 *Mater. Chem. Phys* **120** 566
[9] Shkir M, Abbas H, Kumar S, Bhagavannarayana G and AlFaify S 2014 *J. Phys. Chem. Sol.* **75** 959
[10] Shkir M, AlFaify S, Abbas H and Bhagavannarayana G 2015 *Mater. Chem. Phys.* **155** 36
[11] Azhar S M, Hussaini S S, Shirsat M D, Rabbani G, Shkir M, Alfaify S, Ghramh H A, Baig M I and Anis M 2018 *Mater. Res. Innov.*
[12] Azhar S M, Anis M, Hussaini S S, Kalainathan S, Shirsat M D and Rabbani G 2017 *Opt. Laser Tech.* **87** 11
[13] Dinakaran S, Verma S, Das S J, Bhagavannarayana G, Kar S and Bartwal K 2011 *Appl. Phys. B* **103** 345
[14] Andreetti G D, Cavalca L and Musatti A 1968 *Acta Cryst. B* **24** 683
[15] Williams D J 1984 *Angew. Chem.-Int. Edit.* **23** 690
[16] Shkir M, Riscob B, Khan M A, AlFaify S, Dieguez E and Bhagavannarayana G 2014 *Spectrochem. Acta A* **124** 571
[17] Shkir M, Ganesh V, Vijayan N, Riscob B, Kumar A, Rana D K, Khan M S, Hasmuddin M, Wahab M A and Babu R R 2013 *Spectrochem. Acta A* **103** 199
[18] Bhagavannarayana G, Parthiban S and Meenakshisundaram S 2008 *Cryst. Growth Des.* **8** 446
[19] Meenakshisundaram S, Parthiban S, Sarathi N, Kalavathy R and Bhagavannarayana G 2006 *J. Cryst. Growth* **293** 376
[20] Bhandari S, Sinha N, Ray G and Kumar B 2014 *Chem. Phys. Lett.* **591** 10
[21] Sinha N, Goel N, Singh B K, Gupta M K and Kumar B 2012 *J. Sol. Stat. Chem.* **190** 180
[22] Pahurkar V G, Anis M, Baig M I, Ramteke S P, Babu B and Muley G G 2017 *Optik* **142** 421
[23] Anis M, Muley G G, Pahurkar V G, Baig M I and Dagdale S R 2018 *Mater. Res. Innov.* **22** 99
[24] Dhumane N R, Hussaini S S, Dongre V G and Shirsat M D 2008 *Opt. Mater.* **31** 328
[25] Enculescu M 2010 *Chin. Phys. B* **405** 3722
[26] Raju B, Saritha A, Bhagavannarayana G and Hussain K A 2011 *J. Cryst. Growth* **324** 184
[27] Chandran S, Paulraj R and Ramasamy P 2015 *Mater. Res. Bull.* **68** 210
[28] Zaitseva N, Carman L, Smolsky I, Torres R and Yan M 1999 *J. Cryst. Growth* **204** 512
[29] Hirota S, Miki H, Fukui K and Maeda K 2002 *J. Cryst. Growth* **235** 541
[30] Barbon A, Bellinazzi M, Benedict J B, Brustolon M, Fleming S D, Jang S H, Kahr B and Rohl A L 2004 *Angew. Chem. Int. Ed.* **43** 5328
[31] Wustholz K L, Kahr B and Reid P J 2005 *Phys. Chem. B* **109** 16357
[32] Benedict J B, Wallace P M, Reid P J, Jang S H and Kahr B 2003 *Adv. Mater.* **15** 1068
[33] Yang S M and Ozin G A 2000 *Chem. Comm.* **24** 2507
[34] Wanke M C, Lehmann O, Müller K, Wen Q and Stuke M 1997 *Science* **275** 1284
[35] Kahr B and Gurney R W 2001 *Chem. Rev.* **101** 893

[36] Yadav H, Sinha N, Tyagi N and Kumar B 2015 *Cryst. Growth Des.* **15** 4908
[37] Shkir M 2016 *J. Mater. Res.* **31** 1046
[38] Ushasree P M, Jayavel R, Subramanian C and Ramasamy P 1999 *J. Cryst. Growth* **197** 216
[39] Yahia I S, Farag A, Yakuphanoglu F and Farooq W 2011 *Synthetic Metals* **161** 881
[40] Venkataramanan V, Srinivasan M and Bhat H 1994 *J. Raman Spectros.* **25** 805
[41] Oussaid M, Becker P, Kemiche M and Carabatos-Nédelec C 1998 *Phys. Stat. Sol. B* **207** 103
[42] Samuel B S, Krishnamurthy R and Rajasekaran R 2014 *Spectrochem. Acta A* **132** 526
[43] Kubelka P and Munk F 1931 *Z. Tech. Phys.* **12** 593
[44] Urbach F 1953 *Phys. Rev.* **92** 1324
[45] Shkir M, Riscob B, Ganesh V, Vijayan N, Gupta R, Plaza J, Dieguez E and Bhagavannarayana G 2013 *J. Cryst. Growth* **380** 228
[46] Shakir M, Kushwaha S, Maurya K, Bhagavannarayana G and Wahab M A 2009 *Sol. Stat. Comm.* **149** 2047
[47] Shkir M, Abbas H and Khan Z R 2012 *J. Phys. Chem. Sol.* **73** 1309
[48] Ding Q, Zang X S, Li L, Xu J P, Zhou P, Dong X F and Yan M 2017 *Chin. Phys. B* **26** 67804
[49] Anis M, Ramteke S P, Shirsat M D, Muley G G and Baig M I 2017 *Opt. Mater.* **72** 590
[50] Ramteke S P, Anis M, Baig M I, Shkir M, Ganesh V and Muley G G 2018 *Optik* **158** 634
[51] Azhar S M, Rabbani G, Shirsat M D, Hussaini S S, Baig M I, Ghramh H A and Anis M 2018 *Optik* **165** 259
[52] Xu S, Li G, Chua S, Wang X and Wang W 1998 *Appl. Phys. Lett.* **72** 2451
[53] Kushwaha S, Maurya K, Vijayan N, Gupta A, Haranath D, Kumar B, Kanjilal D and Bhagavannarayana G 2014 *Nucl. Instrum. and Meth. Phys. Res. Sec. B: Beam Interactions with Materials and Atoms* **338** 1
[54] Bol A A, Ferwerda J, Bergwerff J A and Meijerink A 2002 *J. Luminescence* **99** 325
[55] Pal M, Bera S, Sarkar S and Jana S 2014 *RSC Adv.* **4** 11552
[56] Kushwaha S, Maurya K, Haranath D and Bhagavannarayana G 2011 *J. Appl. Cryst.* **44** 1054
[57] Ramteke S P, Anis M, Baig M I and Muley G G 2018 *Optik* **154** 275
[58] Raj S G, Kumar G R, Raghavalu T, Kumar P, Mohan R and Jayavel R 2006 *Spectrochem. Acta A* **65** 1021
[59] Shkir M, Patil P, Arora M, AlFaify S and Algarni H 2017 *Spectrochem. Acta A* **173** 445
[60] Ganesh V, Shkir M, AlFaify S and Yahia I S 2017 *J. Mater. Sci.: Mater. Electron.* **28** 5733
[61] Sankar R, Raghavan C M and Jayavel R 2007 *Cryst. Growth Des.* **7** 501
[62] Dhumane N R, Hussaini S S, Dongre V G, Karmuse P P and Shirsat M D 2009 *Cryst. Res. Technol.* **44** 269
[63] Shkir M, Riscob B and Bhagavannarayana B 2012 *Sol. Stat. Sci.* **14** 773
[64] Anis M, Hussaini S S, Shkir M, Alfaify S, Baig M I and Muley G G 2018 *Optik* **157** 592
[65] Anis M, Muley G G, Baig M I, Hussaini S S and Shirsat M D 2017 *Mater. Res. Innov.* **21** 439
[66] Anis M, Baig M I and Muley G G 2017 *Opt. Mater.* **72** 1
[67] Xue D and Kitamura K 2002 *Sol. Stat. Comm.* **122** 537
[68] Jonscher A K 1977 *Nature* **267** 673
[69] Ramteke S P, Anis M, Pandian M S, Kalainathan S, Baig M I, Ramasamy P and Muley G G 2018 *Opt. Laser Technol.* **99** 197
[70] Baig M I, Anis M, Kalainathan S, Babu B and Muley G G 2017 *Mater. Technol.* **32** 590
[71] Sangwal K 2000 *Mater. Chem. Phys.* **63** 145
[72] Meyer E and Ver Z 1908 *Z. Ver. Dtsch. Ing.* **52** 645
[73] Shkir M, Ganesh V, AlFaify S, Black A, Dieguez E and Bhagavannarayana G 2016 *J. Alloy. Compd.* **686** 438
[74] Hays C and Kendall E 1973 *Metallography* **6** 275
[75] Shkir M, AlFaify S, Ganesh V, Yahia I, Algarni H and Shoukry H 2016 *J. Mater. Sci.: Mater. Electron.* **27** 10673
[76] Riscob B, Shkir M, Ganesh V, Vijayan N, Maurya K, Rao K K and Bhagavannarayana G 2014 *J. Alloy. Compd.* **588** 242